Turbulence Spreading into an Edge Stochastic Magnetic Layer Induced by Magnetic Fluctuation and Its Impact on Divertor Heat Load

M. Kobayashi,[1,2] K. Tanaka,[1,3] K. Ida,[1,2] Y. Hayashi,[1] Y. Takemura,[1] and T. Kinoshita[3]
[1]National Institute for Fusion Science, National Institutes of Natural Sciences, Toki, Gifu 509-5292, Japan
[2]National Institute for Fusion Science, SOKENDAI, The Graduate University for Advanced Studies, Toki, Gifu 509-5292, Japan
[3]Interdisciplinary Graduate School of Engineering Sciences, Kyushu University, Kasuga, Fukuoka 816-8580, Japan

(Received 11 May 2021; revised 20 December 2021; accepted 2 February 2022; published 23 March 2022)

Turbulence spreading into the edge stochastic magnetic layer induced by magnetic fluctuation is observed at the sharp boundary region in the large helical device. The density fluctuation excited at the sharp boundary region with a large pressure gradient does not propagate into the boundary region due to the blocking of turbulence spreading by the large second derivative of the pressure gradient. Once the magnetic fluctuation appears at the boundary, the density fluctuation begins to penetrate the edge stochastic layer and the second derivative of the pressure gradient also decreases. The increase of density fluctuation in this layer results in the broadening and reduction of the peak divertor heat load. It is demonstrated that magnetic fluctuation plays a key role in controlling the turbulence spreading at the boundary of plasma which contributes to the reduction of divertor heat load.

DOI: 10.1103/PhysRevLett.128.125001

The divertor heat load mitigation is a crucial issue for magnetically confined fusion reactors, where the divertor heat flux will increase significantly more than the present-day devices [1]. Control of the power falloff length is, therefore, mandatory [2]. In order to reduce the heat flux, various schemes are being attempted, such as impurity seeding to dissipate the energy via impurity radiation [3,4], magnetic flux expansion of the divertor leg [5], and resonant magnetic perturbation (RMP) field application [6–8] to increase radiation volume and/or to enlarge contact area with the divertor plate.

The turbulence in the scrape-off layer (SOL) has been also recognized as a key player determining SOL width [9–12]. Propagation of the turbulence (turbulence spreading) is important to determine the resulting turbulence profile. Theoretical models of turbulence spreading predict that the turbulence excited at a linearly unstable region can propagate to a region of weaker excitation or to a linearly stable region [13–17]. The process appears as a nonlocality of transport, where the fluctuation level at one place depends on the destabilizing sources located elsewhere [14,15,17,18]. The theoretical model and the numerical simulation predict that the transport barrier formed by flow shear reduces or blocks the turbulence spreading [18,19].

Experimentally, however, direct observation of the turbulence spreading is difficult, because it requires us to distinguish the fluctuations excited locally from those propagated remotely from somewhere else. Although a few experiments observed signature of the turbulence spreading [20–22], there have been no experiments to control the divertor heat load by increasing the turbulence in the SOL region.

In the present experiments, it has been found, for the first time, that the divertor heat load is decreased by the turbulence spreading, which is induced by magnetic fluctuation excited by MHD activity. The large helical device (LHD) has a wide edge stochastic layer, where the plasma density (n_e) and temperature (T_e) are flat due to the magnetic braiding effect [23]. There is, therefore, no turbulence drive in this region. The turbulence is first localized at a steep pressure gradient region, which develops at the confinement boundary. Once the magnetic fluctuation is excited via MHD instability, the turbulence starts spreading into the edge stochastic layer, and the divertor heat load profile is broadened, leading to the reduction of the peak heat load by several factors.

LHD is a heliotron type fusion experiment device with major radius of 3.9 m and averaged minor radius of ~0.6 m [24]. The magnetic field is created by a set of superconducting coils. The magnetic axis $R_{ax} = 3.90$ m, magnetic field strength at the center of the plasma was 2.54 T in the present experiment. The deuterium plasma was sustained with neutral beam injection (NBI) heating of 5 MW. RMP with $m/n = 1/1$ was applied by perturbation coils from the beginning of the discharge, where m and n are the mode number of the poloidal and toroidal Fourier

component of the RMP. The RMP field strength B_r is $B_r/B_0 \sim 0.10\%$, and resonates at radius of ι (rotational transform) $=1$, which is located at the edge region [25,26]. A pronounced edge stochastic layer is created by the RMP application with radial width of $\sim$10 cm as shown in Figs. 1(a) and 1(b) due to the overlapping of magnetic islands of different mode numbers of inherent magnetic islands in the nonaxisymmetric configuration and of those created by the RMP. The global confinement did not degrade by the RMP application in the present experiments. The magnetic field line connection length (L_c) in the stochastic layer is 10^2 to 10^3 m. The L_c increases sharply up to 10^5 m, which is the maximum tracing length in the present calculation, toward the confinement region at $r_{\rm eff} \sim 0.48$ m $r_{\rm eff}$ is defined as a radius of a cylinder that encloses the plasma volume. As seen in Figs. 3(a) and 3(b), T_e and n_e show fairly flat profiles in the stochastic layer, and a steep gradient is formed at the boundary of the confinement region. The beta value during the time window of the analysis was very low, 0.23%, and kept almost constant. The density fluctuation ($\tilde{n}_e$) was measured with a 2D-phase contrast imaging (PCI) system [27,28]. The measured frequency and the wave number ranges are 10 kHz $< f <$ 500 kHz and 0.1 mm^{-1} $< k_\perp <$ 0.8 mm^{-1}, respectively. At the edge region of interest, $k_\perp \rho_s \lesssim 1$. $\rho_s = c_s/\omega_{ci} = 0.2 \sim 1$ mm, is the ion inertial scale length with c_s and ω_{ci} being ion sound speed and ion cyclotron frequency, respectively. The measured fluctuations are, therefore, in the ion scales. The line of sight of the 2D-PCI passes through the entire plasma from top to bottom. The line integrated signal is resolved in space by considering the magnetic field line pitch angle and the propagation direction of the fluctuations perpendicular to the magnetic field lines [27].

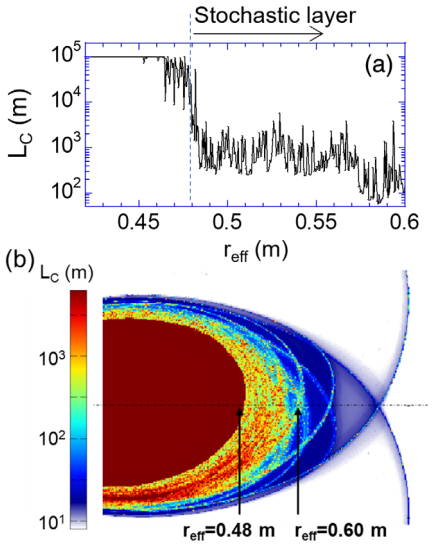

FIG. 1. Radial profiles of (a) L_c in the edge region. (b) 2D distribution of L_c. Corresponding locations of $r_{\rm eff} = 0.48$ and 0.60 m are indicated in (b).

A spectrogram of magnetic probe signal $\tilde{B}_\theta$ and the temporal evolution of the $\tilde{n}_e$ profile in the edge region are shown in Figs. 2(a) and 2(c), respectively. The $\tilde{n}_e$ was normalized with line averaged density $\bar{n}_e$ to compensate the slight increase of $\bar{n}_e$ within the time window. At the initial phase, $t < 4.15$ sec, $\tilde{n}_e$ is localized around $r_{\rm eff} \sim 0.48$ m, which corresponds to the boundary of the confinement region, where steep gradient of T_e and n_e is developed as

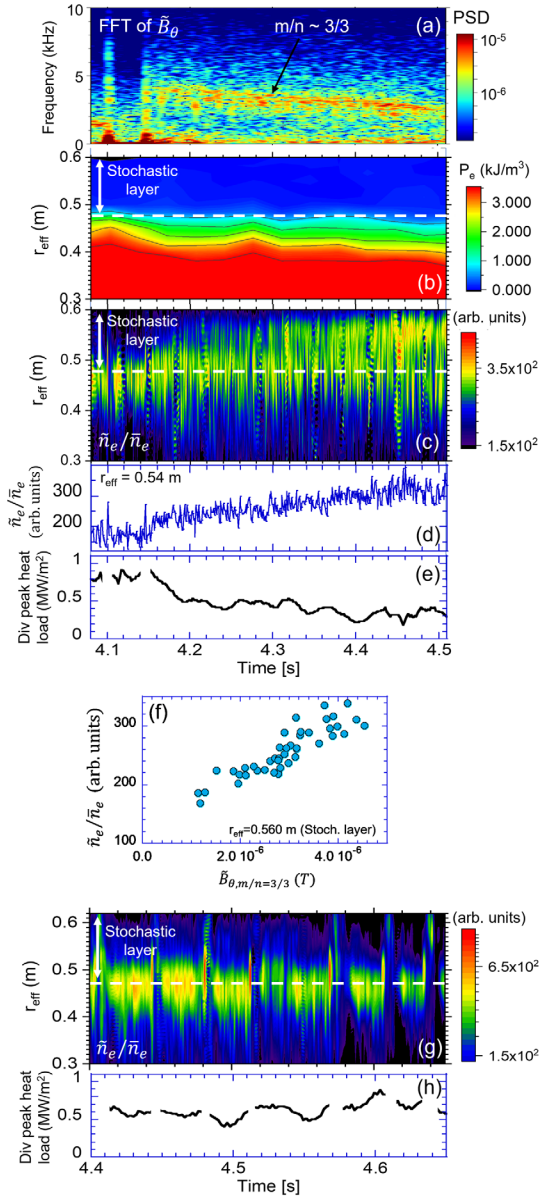

FIG. 2. (a) Spectrogram of magnetic fluctuation, temporal evolutions of radial profiles of (b) P_e and (c) density fluctuation ($\tilde{n}_e$), (d) $\tilde{n}_e$ in the stochastic layer ($r_{\rm eff} = 0.54$ m), (e) divertor peak heat load. (f) $\tilde{n}_e$ in the stochastic layer as a function of the magnetic fluctuation intensity of $m/n = 3/3$ mode (#148584). Time evolutions of (g) radial profiles of $\tilde{n}_e$ and (h) divertor peak heat load in the case without the $m/n = 3/3$ magnetic fluctuation (#148600). The divertor heat load during the MHD burst is masked.

shown in Figs. 3(a) and 3(b). The $k_\perp$ of the fluctuation is in the rage of $0.3-0.5$ mm^{-1} ($k_\perp \rho_i = 0.06-0.1$) with a peak around 0.3 mm^{-1}. The gradient can be a local source of turbulence through various processes such as the ion temperature gradient (ITG) mode or trapped electron mode (TEM), etc. The peak of the density fluctuation spectrum is around 10 kHz. Based on the discussion in Ref. [29] the characteristic is similar to those excited by the ITG turbulence. Strict identification of the turbulence modes is, however, not the main purpose of the present analysis. During the initial phase, MHD bursts occur as indicated by the burst of $\tilde{B}_\theta$ at $t = 4.10$ and 4.15 sec. After the second burst, a coherent mode appears at ~4 kHz and lasts for $t > 4.15$ sec. The mode number of the magnetic fluctuation was identified as $m/n = 3/3$ and it propagates in electron diamagnetic direction in a laboratory frame. There have been no higher harmonics observed of this mode. From the mode number, the fluctuation is considered to be induced by pressure gradient driven MHD instability around $\iota = 1$, where steep gradient is formed at $r_{\rm eff} \approx 0.48$ m as shown in Figs. 3(a) and 3(b). The propagation velocity of the magnetic fluctuation is almost same as the $E \times B$ rotation speed, which is estimated later. After the magnetic fluctuation sets in, $\tilde{n}_e$ begins to spread into the edge stochastic layer as shown in Figs. 2(c) and 2(d). The intensity of the magnetic fluctuation of the mode, $\tilde{B}_{\theta,m/n=3/3}$, gradually increases in time. Figure 2(f) shows $\tilde{n}_e$ in the stochastic layer ($r_{\rm eff} = 0.56$ m) as a function of $\tilde{B}_{\theta,m/n=3/3}$. The $\tilde{n}_e$ in the stochastic layer increases with increasing $\tilde{B}_{\theta,m/n=3/3}$. It is noted that the frequency of $\tilde{B}_{\theta,m/n=3/3}$ is ~4 kHz without harmonics, and is outside of the density fluctuation measurement range as mentioned above. This means that the measured $\tilde{n}_e$ is not directly excited by the magnetic fluctuation. Figures 2(g) and 2(h) show the time evolution of the $\tilde{n}_e$ profile and the peak divertor heat load without the magnetic fluctuation of $m/n = 3/3$ mode with the RMP application. In this case, the turbulence spreading into the stochastic layer does not occur and the divertor peak heat load remains nearly constant. In the series of the experiments, it has been confirmed that the turbulence spreading occurs only when the coherent magnetic fluctuation of the $m/n = 3/3$ mode appears and the spreading never occurs without the coherent magnetic fluctuation.

The physical interpretation of the phenomena is given as follows. Because of the low T_e (<200 eV) and high n_e (>3×10^{19} m^{-3}) in the edge stochastic region, neither charge exchange spectroscopy nor Doppler reflectometer is available for electric field measurements. Nevertheless,

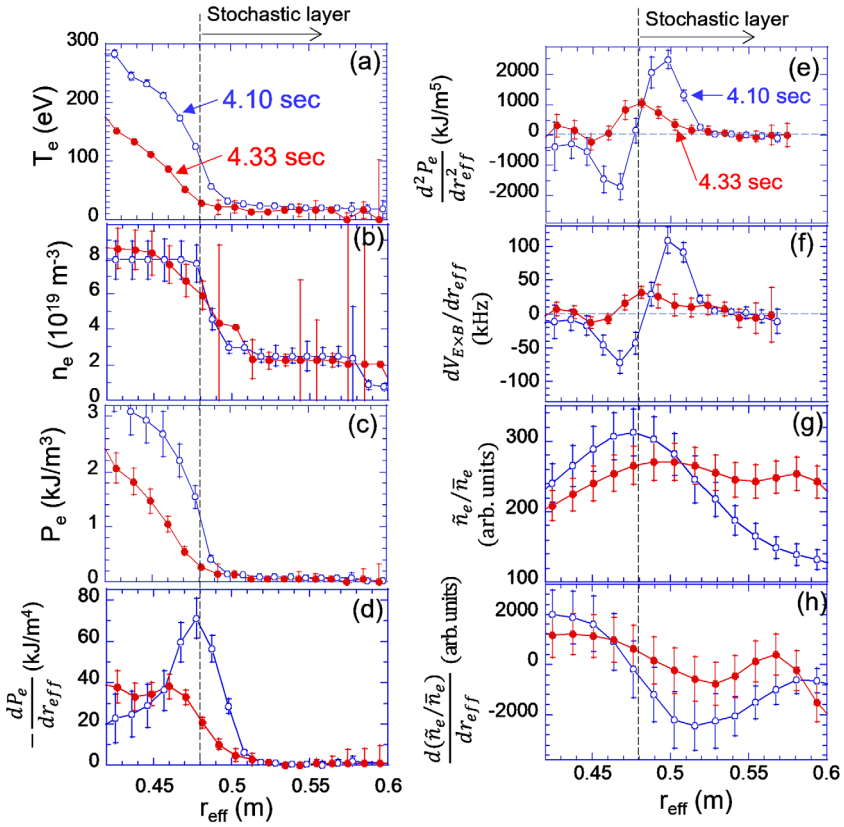

FIG. 3. Radial profiles of (a) T_e, (b) n_e, (c) electron pressure, (d) 1st radial derivative of the pressure, (e) 2nd radial derivative of the pressure, (f) V_{ExB} shearing rate, (g) density fluctuation, and (h) radial derivative of the density fluctuation. Blue (open) symbols: $t = 4.10$ sec, red (closed) symbols: $t = 4.33$ sec (#148584).

the electric field profile can be deduced by assuming force balance in radial direction as, $E_r \approx (\nabla_r p_i / Z_i n_i e)$. The relation is found to be in good agreement with the measured E_r profile in the edge region in stellarators [30] and also in tokamaks [31]. Figure 3 shows radial profiles of T_e, n_e, electron pressure (p_e), its first and second radial derivatives. Because of the low temperature and high density in this region, the equilibration time between electrons and ions, $\tau_T^{ei} = 3.17 \times 10^{14} (A T_e^{1.5} / n_i Z_i^2 ln\Lambda)$ is ~0.5 ms, which is much shorter than the particle duel time in the stochastic layer $\sim L_C / c_s \sim 10$ ms, and than the energy confinement time ~0.1 sec, by 1–2 orders of magnitudes. It is, therefore, considered that $p_e \approx p_i$. Thereby, $\nabla_r p_e$ and $\nabla_r^2 p_e$ in Figs. 3(d) and 3(e) reflect E_r and $\nabla_r E_r \approx \nabla_r (\nabla_r p_i / Z_i n_i e)$ profiles, respectively. At the initial phase, $t = 4.10$ sec, the pressure gradient is steep, ~70 kJ/m^4, and its second derivative takes maxima or minimum of $\sim \pm 2000$ kJ/m^5 [Fig. 3(e)]. Based on the assumption above, this corresponds to radial electric field shear of 300 kV/m^2, and provides $E \times B$ flow ($V_{E\times B}$) shear of ~100 kHz as shown in Fig. 3(f), where the absolute values of the shear takes maximum at both sides of the peak of pressure gradient. On the other hand, after the onset of the magnetic fluctuation, t = 4.33 sec, the pressure gradient becomes weaker and the corresponding $V_{E\times B}$ shear is smaller by several factors. This change of the flow shearing rate suggests that during the initial phase the turbulence generated at the confinement boundary is prevented from propagating by the flow shear as predicted by the models [13,19], while in the later phase with the magnetic fluctuation, the turbulence penetrates to the stochastic layer due to the reduction of the $V_{E\times B}$ shear. This is clearly shown in Figs. 3(g) and 3(h), where the $\tilde{n}_e$ and its radial derivative across the stochastic layer are plotted. At the initial phase, $t = 4.10$ sec, the fluctuation is peaked around $r_{\text{eff}} = 0.48$ m, where the pressure gradient is peaked, too. The fluctuation amplitude decays in both inner and outer directions. In the later phase, however, the radial spreading of the fluctuation is obvious, where the magnitude of the radial derivative decreases in both inner and outer directions.

The results are compared with the global gyrokinetic simulations in Ref. [19], as follows. The flow shearing rate in the initial phase with the turbulence blocking is ~100 kHz, which corresponds to $0.51 c_s/a$, where a is minor radius of plasma. Here c_s/a is used as a measure of turbulence decorrelation rate based on a gyro-Bohm type transport coefficient, $D_{gB} \sim \rho_i^2 c_s / a$. In the later phase with the turbulence spreading the shearing rate decreases and ranges $0.10 \sim 0.21\ c_s/a$. In Ref. [19], the change from turbulence blocking to spreading is found to occur around $0.2\ c_s/a$. The observation of turbulence blocking or spreading in terms of the $V_{E\times B}$ shearing rate is consistent with the predictions of the simulations.

There are two ways for MHD activity to trigger a feedback loop that enhance turbulence spreading. The magnetic fluctuation of $m/n = 3/3$ caused by the MHD activity effectively stochastizes the sharp boundary created by the RMP with $m/n = 1/1$. This is clearly observed in Fig. 2(b), which shows a contour plot of temporal evolution of radial pressure profile (p_e). After the MHD mode excitation the sharp boundary is lost around $r_{\text{eff}} = 0.48$ m, leading to reduction of the second derivative of p_e and to reduction of the $V_{E\times B}$ shear. Since the shear flow reduction loses the screening effect of the magnetic perturbation field, it results in further stochastization as observed in Ref. [32]. The process drives the feedback loop between the stochastization, loss of sharp boundary, and $V_{E\times B}$ shear reduction. At the same time, the reduced $V_{E\times B}$ shear loses its capability of blocking the turbulence. Then, the enhanced turbulence spreading weakens the sharp boundary, $\nabla^2 p$. This leads to $V_{E\times B}$ shear reduction. The process also drives the feedback loop that enhances the turbulence spreading. In addition, the MHD activity can trigger directly turbulence spreading through nonlinear coupling with the background turbulence as observed in HL-2A [33]. Such a process also can trigger the feedback loop that enhances the turbulence spreading.

During the turbulence spreading phase, reduction of the peak divertor heat load is observed as shown in Fig. 2(e), which is measured by the Langmuir probe array at the divertor plate. The heat load profile normalized by the peak values is shown in Fig. 4(a) together with L_c on the divertor plate in Fig. 4(b). The heat load is localized at the long L_c region of ~10^3 m, and rapidly decays into the short L_c region. The heat load profile becomes broad in the turbulence spreading phase at $t = 4.40$ sec. The peak heat load is plotted as a function of the $\tilde{n}_e$ in the stochastic layer in Fig. 4(c), together with the FWHM of the divertor heat load profile in Fig. 4(d). The FWHM was obtained by fitting with a Gaussian function. As the fluctuation increases in the stochastic layer, the peak heat load decreases by a factor of 3 to 4 with concomitant broadening of the profile. Figure 4(g) plots the divertor peak heat load as a function of the edge pressure gradient at $r_{\text{eff}} = 0.47 - 0.49$ m before and after the turbulence spreading. The dashed line represents a linear fit to the data before the spreading. The peak heat load after the spreading clearly deviates from the linear scaling, indicating an impact of the turbulence spreading on the peak heat load.

The global confinement is maintained during the turbulence spreading phase, as shown in Fig. 4(e), where the plasma stored energy is plotted as a function of $\tilde{n}_e$ in the stochastic layer. This is caused by core-edge coupling, where the pressure profile peaks at central region while the edge pressure gradient degrades during the spreading. Similar core-edge coupling has been observed in the EAST tokamak, where core pressure increases to compensate the pedestal pressure degradation [34]. In the LHD, the transport is more dominated by turbulence than neoclassical transport as the radial electric field increases [35], the

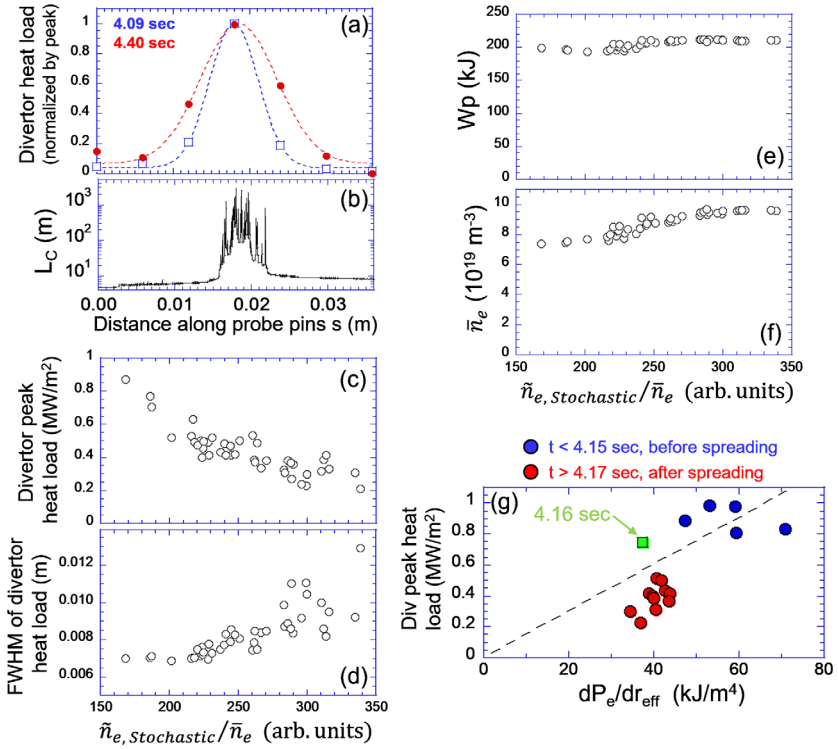

FIG. 4. (a) Divertor heat load profile normalized by the peak values, fitted with a Gaussian function (dotted lines). (b) L_c profile at the divertor plate. Blue (open) symbols: $t = 4.09$ sec, before the turbulence spreading. Red (closed) symbols: $t = 4.40$ sec, after the turbulence spreading. The peak heat load are 0.81 and 0.23 MW/m^2 at 4.10 and 4.40 sec, respectively. (c) Divertor peak heat load, (d) the FWHM of the heat load profile, (e) Wp, and (f) $\bar{n}_e$, as a function of density fluctuation in the stochastic layer ($r_{\mathrm{eff}} = 0.56$ m). (g) Divertor peak heat load as a function of the edge pressure gradient at $r_{\mathrm{eff}} = 0.47 - 0.49$ m. Blue circles: $t < 4.15$ sec, before turbulence spreading, red circles: $t > 4.17$ sec, after turbulence spreading, green square, $t = 4.16$ sec. The dashed line shows a linear fit to the data before the spreading ($t < 4.15$ sec).

situation of which applies to the present experiments. The mechanism of the core-edge coupling is beyond of the scope of this paper and is left for future work.

The results show the peak divertor heat load reduction caused by the turbulence spreading while the core performance is maintained.

In summary, we have observed clear evidence of turbulence spreading into the edge stochastic magnetic layer, where no drive for turbulence exists due to the flat T_e and n_e profiles. Density fluctuation is localized at the boundary of the confinement region, where a steep pressure gradient develops to provide an energy source for turbulence. Once the magnetic fluctuation is excited at the gradient region, the density fluctuation spreads into the stochastic layer. The density fluctuation enhancement in the stochastic layer leads to widening of the divertor heat load profile and to reduction of the peak heat load as evidence of enhanced cross-field energy transport in the stochastic layer caused by the turbulence spreading. The role of the magnetic fluctuation on the turbulence spreading is considered to be the stochastization of the boundary of the confinement region, which results in a loss of the sharp boundary and thus leads to reduction of the $V_{E\times B}$ shearing rate to block the spreading. The results demonstrated a new scheme to control the divertor heat load with magnetic fluctuation induced by MHD activity that leads to the enhancement of turbulence in the SOL region.

The LHD data can be accessed from the LHD data repository at https://www-lhd.nifs.ac.jp/pub/Repository_en.html.

The authors would like to thank the LHD Experiment group for their excellent work on the operation of LHD. This work was financially supported by JSPS KAKENHI Grants No. 19H01878 and No. 21H04458.

[1] N. Asakura *et al.*, Nucl. Fusion **57**, 126050 (2017).
[2] K. Ida *et al.*, Nucl. Fusion **59**, 117001 (2019).
[3] F. Effenberg *et al.*, Nucl. Fusion **59**, 106020 (2019).
[4] K. Mukai, S. Masuzaki, Y. Hayashi, T. Oishi, C. Suzuki, M. Kobayashi, H. Tanaka, and B. J. Peterson, Plasma Fusion Res. **15**, 1402051 (2020).
[5] C. Theiler *et al.*, Nucl. Fusion **57**, 072008 (2017).
[6] Y. In, A. Loarte, H. H. Lee, K. Kim, Y. M. Jeon, J.-K. Park, J.-W. Ahn, G. Y. Park, M. Kim, and H. Park, Nucl. Fusion **59**, 126045 (2019).

[7] M. Faitsch, B. Sieglin, D. Brida, W. Suttrop, T. Lunt, T. Eich, and M. Wischmeier, Plasma Phys. Controlled Fusion **61**, 014008 (2019).
[8] A. B. Briesemeister *et al.*, Nucl. Fusion **57**, 076038 (2017).
[9] Ph. Ghendrih, Y. Sarazin, G. Ciraolo, G. Darmet, X. Garbet, V. Grangirard, P. Tamain, S. Benkadda, and P. Beyer, J. Nucl. Mater. **363–365**, 581 (2007).
[10] J. R. Myra, D. A. Russell, D. A. D'Ippolito, J.-W. Ahn, R. Maingi, R. J. Maqueda, D. P. Lundberg, D. P. Stotler, S. J. Zweben, and M. Umansky, J. Nucl. Mater. **415**, S605 (2011).
[11] P. Manz, T. T. Ribeiro, B. D. Scott, G. Birkenmeier, D. Carralero, G. Fuchert, S. H. Müller, H. W. Müller, U. Stroth, and E. Wolfrum, Phys. Plasmas **22**, 022308 (2015).
[12] C. S. Chang *et al.*, Nucl. Fusion **57**, 116023 (2017).
[13] N. Mattor and P. H. Diamond, Phys. Rev. Lett. **72**, 486 (1994).
[14] X. Garbet, L. Laurent, A. Samain, and J. Chinardet, Nucl. Fusion **34**, 963 (1994).
[15] T. S. Hahm, P. H. Diamond, Z. Lin, K. Itoh, and S.-I. Itoh, Plasma Phys. Controlled Fusion **46**, A323 (2004).
[16] Oe. D. Guercan, P. H. Diamond, T. S. Hahm, and Z. Lin, Phys. Plasmas **12**, 032303 (2005).
[17] K. Ida *et al.*, Adv. Phys. **5**, 1801354 (2020).
[18] T. S. Hahm, Y. J. Kim, P. H. Diamond, and G. J. Choi, Phys. Plasmas **28**, 022302 (2021).
[19] W. X. Wang, T. S. Hahm, W. W. Lee, G. Rewoldt, J. Manickam, and W. M. Tang, Phys. Plasmas **14**, 072306 (2007).
[20] T. Estrada, C. Hidalgo, and T. Happel, Nucl. Fusion **51**, 032001 (2011).
[21] G. Grenfell, B. Ph. van Milligen, U. Losada, W. Ting, B. Liu, C. Silva, M. Spolaore, and C. Hidalgo, Nucl. Fusion **59**, 016018 (2019).
[22] K. Ida, T. Kobayashi, T. Tokuzawa, T. Akiyama, H. Tanaka, M. Yoshinuma, and K. Itoh, Nucl. Fusion **58**, 112008 (2018).
[23] A. B. Rechester and M. N. Rosenbluth, Phys. Rev. Lett. **40**, 38 (1978).
[24] Y. Takeiri *et al.*, Nucl. Fusion **57**, 102023 (2017).
[25] M. Kobayashi *et al.*, Nucl. Fusion **59**, 096009 (2019).
[26] K. Tanaka *et al.*, Plasma Fusion Res. **8**, 2402141 (2013).
[27] K. Tanaka, C. A. Michael, L. N. Vyacheslavov, A. L. Sanin, K. Kawahata, T. Akiyama, T. Tokuzawa, and S. Okajima, Rev. Sci. Instrum. **79**, 10E702 (2008).
[28] C. A. Michael, K. Tanaka, L. Vyacheslavov, A. Sanin, and K. Kawahata, Rev. Sci. Instrum. **86**, 093503 (2015).
[29] K. Ida, M. Yoshinuma, K. Tanaka, M. Nakata, T. Kobayashi, Y. Fujiwara, R. Sakamoto, G. Motojima, and S. Masuzaki, Nucl. Fusion **61**, 016012 (2021).
[30] H. Ehmler, Y. Turkin, C. D. Beidler, H. Maaßberg, A. Dinklage, and T. Klinger (W7-AS Team), Nucl. Fusion **43**, L11 (2003).
[31] J. Schmirmer, G. D. Conway, H. Zohm, and W. Suttrop (the ASDEX Upgrade Team), Nucl. Fusion **46**, S780 (2006).
[32] K. Ida, M. Yoshinuma, H. Tsuchiya, T. Kobayashi, C. Suzuki, M. Yokoyama, A. Shimizu, K. Nagaoka, S. Inagaki, and K. Itoh, Nucl. Fusion **57**, 076032 (2017).
[33] W. Chen, Y. Xu, X. T. Ding, Z. B. Shi, M. Jiang, W. L. Zhong, and X. Q. Ji, Nucl. Fusion **56**, 044001 (2016).
[34] L. Wang *et al.*, Nat. Commun. **12**, 1365 (2021).
[35] K. Ida *et al.*, Phys. Rev. Lett. **86**, 5297 (2001).